

# NGTS-14Ab: a Neptune-sized transiting planet in the desert

A. M. S. Smith<sup>1,\*</sup>, J. S. Acton<sup>2</sup>, D. R. Anderson<sup>3,4</sup>, D. J. Armstrong<sup>3,4</sup>, D. Bayliss<sup>3,4</sup>, C. Belardi<sup>2</sup>, F. Bouchy<sup>5</sup>, R. Brahm<sup>6,7</sup>, J. T. Briegal<sup>8</sup>, E. M. Bryant<sup>3,4</sup>, M. R. Burleigh<sup>2</sup>, J. Cabrera<sup>1</sup>, A. Chaushev<sup>9</sup>, B. F. Cooke<sup>3,4</sup>, J. C. Costes<sup>10</sup>, Sz. Csizmadia<sup>1</sup>, Ph. Eigmüller<sup>1</sup>, A. Erikson<sup>1</sup>, S. Gill<sup>3,4</sup>, E. Gillen<sup>8,11,12</sup>, M. R. Goad<sup>2</sup>, M. N. Günther<sup>13,14</sup>, B. A. Henderson<sup>2</sup>, A. Hogan<sup>2</sup>, A. Jordán<sup>6,7</sup>, M. Lendl<sup>5</sup>, J. McCormac<sup>3,4</sup>, M. Moyano<sup>15</sup>, L. D. Nielsen<sup>5</sup>, H. Rauer<sup>1,9,16</sup>, L. Raynard<sup>2</sup>, R. H. Tilbrook<sup>2</sup>, O. Turner<sup>5</sup>, S. Udry<sup>5</sup>, J. I. Vines<sup>17</sup>, C. A. Watson<sup>10</sup>, R. G. West<sup>3,4</sup>, and P. J. Wheatley<sup>3,4</sup>

<sup>1</sup> Institute of Planetary Research, German Aerospace Center, Rutherfordstrasse 2, 12489 Berlin, Germany

<sup>2</sup> School of Physics and Astronomy, University of Leicester, LE1 7RH, UK

<sup>3</sup> Centre for Exoplanets and Habitability, University of Warwick, Gibbet Hill Road, Coventry CV4 7AL, UK

<sup>4</sup> Dept. of Physics, University of Warwick, Gibbet Hill Road, Coventry CV4 7AL, UK

<sup>5</sup> Observatoire de Genève, Université de Genève, 51 Ch. des Maillettes, 1290 Sauverny, Switzerland

<sup>6</sup> Facultad de Ingeniería y Ciencias, Universidad Adolfo Ibáñez, Av. Diagonal las Torres 2640, Peñalolén, Santiago, Chile

<sup>7</sup> Millennium Institute for Astrophysics, Santiago, Chile

<sup>8</sup> Astrophysics Group, Cavendish Laboratory, J.J. Thomson Avenue, Cambridge CB3 0HE, UK

<sup>9</sup> Center for Astronomy and Astrophysics, TU Berlin, Hardenbergstr. 36, D-10623 Berlin, Germany

<sup>10</sup> Astrophysics Research Centre, School of Mathematics and Physics, Queen's University Belfast, BT7 1NN Belfast, UK

<sup>11</sup> Astronomy Unit, Queen Mary University of London, Mile End Road, London E1 4NS, UK

<sup>12</sup> Winton Fellow

<sup>13</sup> Department of Physics, and Kavli Institute for Astrophysics and Space Research, Massachusetts Institute of Technology, 77 Mass. Ave, Cambridge, MA 02139, USA

<sup>14</sup> Juan Carlos Torres Fellow

<sup>15</sup> Instituto de Astronomía, Universidad Católica del Norte, Angamos 0610, 1270709, Antofagasta, Chile

<sup>16</sup> Institute of Geological Sciences, FU Berlin, Malteserstr. 74-100, D-12249 Berlin, Germany

<sup>17</sup> Departamento de Astronomía, Universidad de Chile, Casilla 36-D, Santiago, Chile

Received 19 October 2020; accepted 24 December 2020

## ABSTRACT

**Context.** The sub-Jovian or Neptunian desert is a previously-identified region of parameter space where there is a relative dearth of intermediate-mass planets at short orbital periods.

**Aims.** We present the discovery of a new transiting planetary system within the Neptunian desert, NGTS-14A.

**Methods.** Transits of NGTS-14Ab were discovered in photometry from the Next Generation Transit Survey (NGTS). Follow-up transit photometry was conducted from several ground-based facilities, as well as extracted from TESS full-frame images. We combine radial velocities from the HARPS spectrograph with the photometry in a global analysis to determine the system parameters.

**Results.** NGTS-14Ab has a radius about 30 per cent larger than that of Neptune ( $0.444 \pm 0.030 R_{\text{Jup}}$ ), and is around 70 per cent more massive than Neptune ( $0.092 \pm 0.012 M_{\text{Jup}}$ ). It transits the main-sequence K1 star, NGTS-14A, with a period of 3.54 days, just far enough to have maintained at least some of its primordial atmosphere. We have also identified a possible long-period stellar mass companion to the system, NGTS-14B, and we investigate the binarity of exoplanet host stars inside and outside the Neptunian desert using Gaia.

**Key words.** planetary systems – Planets and satellites: detection – Planets and satellites: individual: NGTS-14Ab – binaries: general

## 1. Introduction

The first generation of wide-field transit surveys, the most prolific of which were SuperWASP (Pollacco et al. 2006) and HAT-Net (Bakos et al. 2002), unveiled the rich diversity of hot Jupiters. These planets, although intrinsically rare, have been discovered in numbers large enough to enable statistical population analyses such as those investigating inflation (e.g. Thorngren & Fortney 2018; Sestovic et al. 2018). Transiting hot Jupiters also remain the best-studied individual planetary systems, with characterisation observations such as atmospheric transmission spectroscopy pioneered on these objects (e.g. Sing et al. 2016).

The Kepler (Borucki et al. 2010) and K2 (Howell et al. 2014) missions, and the ongoing TESS (Transiting Exoplanet Survey Satellite; Ricker et al. 2015) mission subsequently revealed a large population of small (less than 2 – 3 Earth radii), short-period planets. In between these two populations, however, lies a relatively unpopulated region of parameter space, often referred to as the sub-Jovian or Neptunian desert (Szabó & Kiss 2011; Mazeh et al. 2016).

The Next Generation Transit Survey (NGTS; Wheatley et al. 2018) consists of twelve independent 0.2-m telescopes, each equipped with a red-sensitive  $2k \times 2k$  CCD covering eight square degrees. The survey is optimised for detecting short-period planets transiting K-dwarf stars, with the goal of detecting Neptune-sized planets. One of the main drivers for the extremely

\* e-mail: alexis.smith@dlr.de

high-precision photometry achieved by NGTS is the telescope guiding, which uses DONUTS (McCormac et al. 2013) to ensure sub-pixel pointing precision throughout the duration of an observing season. This has allowed the detection of significantly shallower transits than previously achieved from the ground, and the discovery of planets in the Neptunian desert, such as NGTS-4b (West et al. 2019).

In this paper we report the discovery from NGTS of a transiting planet slightly larger than Neptune orbiting the early K-dwarf NGTS-14A. In Section 2, we present the host star, and show that it probably has a bound long-period M-dwarf companion. In Section 3 we present our observations of the system with both NGTS and other facilities. In Section 4 we characterise the host star, and in Section 5 we perform a joint analysis of the transit photometry and radial velocities to determine the system parameters. Finally, we discuss NGTS-14 in the context of the Neptunian desert in Section 6, and summarise our findings in Section 7.

## 2. NGTS-14B

We list in Table 1 the Gaia positions, proper motions and parallaxes (Gaia Collaboration et al. 2018) for both NGTS-14A and NGTS-14B, a fainter star which lies just 3.59 arcseconds away (see Fig. 1). The parallaxes of the two objects are identical to much less than  $1 \sigma$  significance, and the proper motions in the RA direction are compatible at the  $2 \sigma$  level. We note, however, that in the Declination direction, the proper motions differ from each other with a significance of  $5.7 \sigma$ . We conclude, however, that these two stars are co-moving, and likely to be gravitationally bound.

As a test of the statistical significance of finding a companion with similar parallax and proper motions close to our target, we searched the Gaia DR2 catalogue for all stars lying within  $5^\circ$  of NGTS-14A<sup>1</sup> and whose proper motions and parallax match those of NGTS-14A to within  $6 \sigma$ . This search of an area  $2.5 \times 10^7$  times larger than the area defined by a radius equal to the separation between target and putative companion returned exactly 100 results, excluding NGTS-14A itself. This implies that the chance of finding such an object within  $3''.6$  is around  $4 \times 10^{-6}$ .

At a distance of  $316.7 \pm 4.8$  pc, the projected separation of the two stars implies a physical separation of  $1137 \pm 17$  au. If the two objects are gravitationally bound, this sets a lower limit to the binary orbital period of around 40 000 yr, assuming a circular orbit. For a moderately eccentric orbit (0.6), this lower limit is reduced to around 20 000 yr, which is the orbital period obtained if we assume that we are observing NGTS-14B at apastron. We note that the physical separation implied here is an order of magnitude smaller than the widest binary that can survive for  $\sim 10$  Gyr in the Solar neighbourhood (Jiang & Tremaine 2010).

We also note that at a distance of around 320 pc, the apparent discrepancy in proper motions in the declination direction ( $1.1 \pm 0.2 \text{ mas yr}^{-1}$ ) corresponds to a physical velocity of around  $1.5 \text{ km s}^{-1}$ , which could be easily explained by the orbital motion of the secondary with respect to the primary. We searched the Digitized Sky Survey for archival imaging, but we found no images with sufficient angular resolution to resolve the two sources. A radial velocity measurement of NGTS-14B would provide further evidence of whether or not the two stars are really a binary

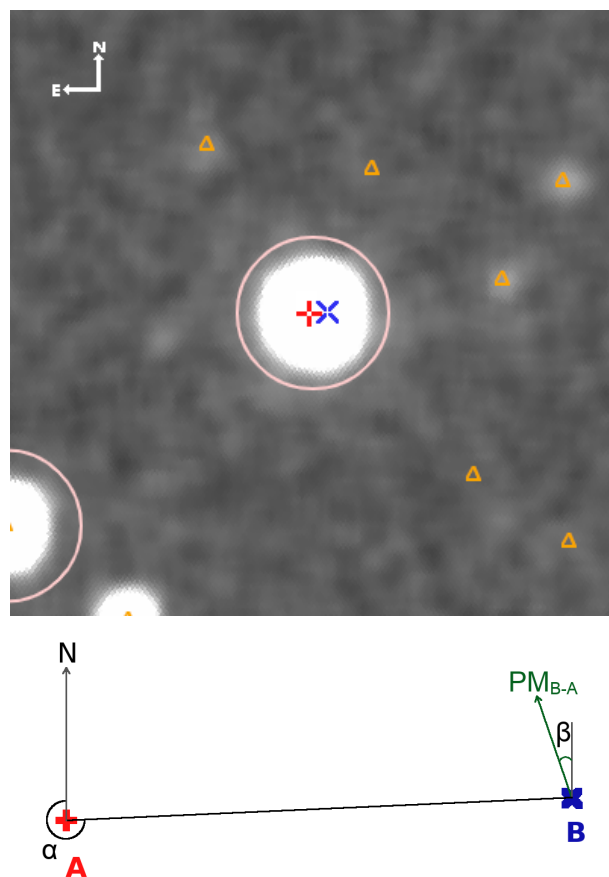


**Fig. 1.** Upper panel: NGTS deep stacked image ( $2' \times 2'$ ) centred on NGTS-14A. The Gaia positions of NGTS-14A and NGTS-14B are indicated with a red '+' and a blue 'x', respectively. The pink circle indicates the NGTS photometric aperture, which has a radius of 3 pixels ( $15''$ ). Other Gaia sources are marked with orange triangles. North is up, and East to the left. Lower panel: Sketch of NGTS-14, showing the separation of NGTS-14A and NGTS-14B, which are represented by the same symbols as in the upper panel. NGTS-14B lies on a bearing  $\alpha = 267.49$  degrees from NGTS-14A. The direction of the relative proper motion of NGTS-14B with respect to NGTS-14A is indicated with the green arrow. The bearing of this proper motion vector is  $\beta = 18.8 \pm 9.5$  degrees, and its magnitude is  $1.18 \pm 0.20 \text{ mas yr}^{-1}$ .

pair, but NGTS-14B is too faint to be observed with CORALIE or HARPS (See Section 3.3).

The existence of such binary companions to planet host stars is interesting, since even at these very large separations, a binary companion may influence the evolution of the planet. For instance, long-period outer companions can act to maintain a non-zero planetary orbital eccentricity, even for short-period planets whose orbits would otherwise be rapidly circularised through tidal interactions with the host star (e.g. Wu & Murray 2003).

NGTS-14B is  $4.098 \pm 0.004$  magnitudes fainter than NGTS-14A in the  $G$ -band, and  $2.17 \pm 0.08$  magnitudes fainter in the  $K$ -band. The spectral type of NGTS-14A is estimated to be K1V, based on the effective temperature derived from spectral analysis, and the tabulation of Pecaat & Mamajek 2013<sup>2</sup>.

Based on the absolute  $G$ -band magnitudes in the aforementioned table, if NGTS-14A has a spectral type of K1V, then NGTS-14B is probably an M2.5V star. Alternatively, using the ( $G$ - $K$ ) colour, the best-matching spectral types (according to the

<sup>1</sup> Gaia DR2 reports a total of  $4.78 \times 10^5$  sources within  $5^\circ$  of NGTS-14A.

<sup>2</sup> [http://www.pas.rochester.edu/~emamajek/EEM\\_dwarf\\_UBVIJHK\\_colors\\_Teff.txt](http://www.pas.rochester.edu/~emamajek/EEM_dwarf_UBVIJHK_colors_Teff.txt)

mentioned table) are K1.5V and M3.5V for NGTS-14A and NGTS-14B, respectively. We adopt spectral types of K1V and M3V for the two stars, and account for the flux contamination of NGTS-14B in our light curves (Sec. 5.1).

### 3. Observations

#### 3.1. NGTS photometry

NGTS-14A lies in one of the fields observed by NGTS starting from the commencement of routine science operations in 2016 April. In all, a total of 220 829 observations were made of this field using a single NGTS telescope, between 2016 April 21 and 2016 December 22. Each image has an exposure time of 10 s, and a typical cadence of 13 s. The data were reduced using the NGTS pipeline (Wheatley et al. 2018), which comprises standard bias subtraction and flat-field correction, followed by aperture photometry based on the CASUtools<sup>3</sup> software package. Finally, systematic effects in the light curves were removed using the SYSREM algorithm (Tamuz et al. 2005).

The NGTS light curves are searched for period transit-like signals using our implementation of the box-fitting least-squares (BLS) algorithm (Kovács et al. 2002). In the case of NGTS-14A, a signal consistent with a transiting exoplanet was detected, with a periodicity of around 3.5 days. After passing several vetting checks designed to eliminate false positives such as eclipsing binaries and blended systems (e.g. Günther et al. 2017), we initiated follow-up observations to confirm the planetary nature of the system, and to better characterise it.

We also note that this system received a high planetary probability of 0.97 from a neural network trained to distinguish between transiting planetary systems and false positives in NGTS data (Chaushev et al. 2019).

#### 3.2. Follow-up photometry

We used several larger aperture telescopes, as well as multiple NGTS telescopes, to perform follow-up transit observations. The motivation of these observations was to confirm the transit, increase the signal-to-noise of our transit photometry to improve the characterisation of the system, and to improve our knowledge of the orbital ephemeris by extending the observational baseline.

##### 3.2.1. SAAO 1-m

We observed a partial transit of NGTS-14Ab on the night of 2019 October 04, from the South African Astronomical Observatory in Sutherland, Northern Cape using their 1-m telescope. The telescope was equipped with one of the Sutherland High-speed Optical Cameras (SHOC; specifically ‘SHOC’n’awe’). A description of the instrument can be found in Coppejans et al. (2013). The observations were conducted in I-band, in focus, with  $4 \times 4$  binning of the CCD, and each of the 960 exposures had a duration of 20 s.

The data were bias and flat field corrected via the standard procedure, using the SAFPHOT Python package (Chaushev & Raynard, in preparation). Differential photometry was also carried out using SAFPHOT, by first extracting aperture photometry for both the target and comparison stars using the SEP package (Barbary 2016). The sky background was measured and subtracted using the SEP background map, adopting box size and fil-

ter width parameters that minimised background residuals, measured across the frame after masking the stars. Three comparison stars were then utilised to perform differential photometry on the target, using a 3.4 pixel ( $0''.57$ ) radius aperture which maximised the signal-to-noise.

##### 3.2.2. EulerCam

A partial transit of NGTS-14Ab was observed on the night of 2019 August 08 with EulerCam on the 1.2-m Euler-Swiss telescope at La Silla Observatory, Chile. A total of 271 observations were made in a filter corresponding to the NGTS bandpass, each with an exposure time of 40 s, giving a cadence of around 52 s. A slight defocus was applied during the observations. Standard data reduction and aperture photometry techniques were applied, using a photometric aperture radius of 19 pixels ( $= 4''.085$ ), and 17 comparison stars.

##### 3.2.3. CHAT

Another partial transit of NGTS-14Ab was observed from the Chilean-Hungarian Automated Telescope (CHAT), a 0.7-m robotic telescope installed at Las Campanas Observatory, Chile. The observations were conducted on the night of 2019 November 8, using an  $i'$  filter. The cadence of the light curve is around 180 s and 73 images were obtained spanning airmass values between 1 and 2. Data was processed with a dedicated pipeline adapted from a set of routines to process photometric data of the LCOGT network (e.g. Hartman et al. 2019; Espinoza et al. 2019; Jordán et al. 2019).

##### 3.2.4. NGTS multi-telescope observations

In addition to its survey mode, where each telescope observes a different field to maximise sky coverage, NGTS can also be operated in a mode where multiple telescopes observe the same target simultaneously (Smith et al. 2020). This mode is used for follow-up of shallow transits detected by the NGTS survey, as well as for TESS targets (Jenkins et al. 2020; Armstrong et al. 2020) and for other exoplanets transiting bright stars (Bryant et al. 2020).

We observed a partial transit of NGTS-14Ab on the night of 2019 November 08 (the same event we observed with CHAT), using eight of the NGTS telescopes. We obtained a total of 8790 exposures (around 1100 per camera), each with the usual NGTS exposure time (10 s) and cadence (13 s).

The NGTS follow-up data for NGTS-14A were reduced using a custom photometry pipeline. This pipeline uses the SEP Python library for both the source extraction and the aperture photometry (Bertin & Arnouts 1996; Barbary 2016). We do not apply bias, dark, and flat-field image corrections during the image reduction, as testing showed them to provide no improvement to the photometric precision achieved. We use Gaia (Gaia Collaboration et al. 2018) to automatically identify comparison stars with a similar colour, brightness and CCD position to NGTS-14A (see Bryant et al. 2020, for more details on the photometric pipeline).

##### 3.2.5. TESS

NGTS-14A falls in Sector 1 of the TESS survey, which was observed between 2018 July 25 and 2018 August 22, covering seven transits of NGTS-14Ab. We were able to extract a light curve from the full-frame images (FFIs) of Camera 1, CCD 2,

<sup>3</sup> <http://casu.ast.cam.ac.uk/surveys-projects/software-release>

**Table 1.** Catalogue information for NGTS-14A and NGTS-14B.

Positions & proper motions	NGTS-14A	NGTS-14B	Source
RA (J2015.5)	21h54m04.20s	21h54m03.89s	Gaia
Dec (J2015.5)	-38° 22' 38".71	-38° 22' 38".55	Gaia
pmRA (mas yr <sup>-1</sup> )	-23.662 ± 0.042	-23.282 ± 0.191	Gaia
pmDec (mas yr <sup>-1</sup> )	5.488 ± 0.034	6.602 ± 0.192	Gaia
parallax (mas)	3.076 ± 0.034	3.088 ± 0.176	Gaia
Projected separation from NGTS-14A	–	3".59016 ± 0".00015	Gaia
Distance from Earth (pc) <sup>†</sup>	316.7 ± 4.8	316 ± 18	
<b>Magnitudes</b>			
<i>B</i> (Johnson)	14.093 ± 0.055	–	APASS
<i>V</i> (Johnson)	13.237 ± 0.078	–	APASS
<i>G</i> (Gaia)	13.0986 ± 0.0006	17.197 ± 0.004	Gaia
<i>BP</i> (Gaia)	13.5448 ± 0.0014	18.147 ± 0.060	Gaia
<i>RP</i> (Gaia)	12.5095 ± 0.0008	15.947 ± 0.020	Gaia
<i>g'</i> (Sloan)	13.607 ± 0.084	–	APASS
<i>r'</i> (Sloan)	12.989 ± 0.054	–	APASS
<i>i'</i> (Sloan)	12.751 ± 0.056	–	APASS
TESS	12.5638 ± 0.006	16.211 ± 0.014	TESS
<i>J</i>	11.813 ± 0.029	≥ 12.431 (2 $\sigma$ limit)	2MASS
<i>H</i>	11.386 ± 0.037	≥ 11.859 (2 $\sigma$ limit)	2MASS
<i>K</i>	11.305 ± 0.027	13.474 ± 0.070	2MASS
<i>W1</i>	11.148 ± 0.022	–	WISE
<i>W2</i>	11.212 ± 0.020	–	WISE
<i>W3</i>	11.334 ± 0.166	–	WISE
Spectral type	K1V	M3V	Sec. 2
<b>Additional identifiers:</b>			
Gaia DR2	6585082036193768832	6585082036193769088	
2MASS J	21540423-3822388	21540393-3822386	
TIC	197643976	197641898	

Gaia: Gaia DR2 (Gaia Collaboration et al. 2016, 2018)

APASS: AAVSO Photometric all-sky survey DR9 (Henden et al. 2016)

2MASS: The Two Micron All Sky Survey (Skrutskie et al. 2006)

WISE: Wide-field Infrared Survey Explorer (Cutri & et al. 2013)

<sup>†</sup>Calculated from Gaia DR2 parallax, incorporating the systematic offset of Stassun & Torres (2018)

which have a cadence of 30 minutes. To do this, we used a custom photometric aperture selected on the basis of a flux threshold, and to minimise blending from other sources. A  $15 \times 15$  pixels area was used for background estimation.

We ran the BLS algorithm on the TESS data to test if the planet could have been detected from the TESS data alone. A peak at around 3.5 d is the highest in the resulting periodogram, with a significance (following Collier Cameron et al. 2006) of 10.9. This suggests that an exhaustive search of light curves derived from the TESS FFIs could have revealed this system. However the transit is much less evident in TESS data compared with the NGTS data. This is primarily due to the fact that NGTS typically produces higher precision photometry for stars with  $T > 12.5$ .

The transit photometry from all the instruments listed above is listed in Table 2, and shown in Fig. 3.

### 3.3. High resolution spectroscopy

#### 3.3.1. CORALIE

We observed NGTS-14A with the CORALIE spectrograph on the Swiss 1.2 m Euler telescope at La Silla Observatories, Chile (Queloz et al. 2001b), between 3 November and 4 December 2018. CORALIE has a resolving power of  $R \sim 60\,000$  and is

**Table 2.** Photometry of NGTS-14A. The full table is available at the CDS. Only a few lines are shown here for guidance on the format. Note that the fitted offsets between datasets are not applied here, and nor is our correction for contamination from NGTS-14B.

BJD <sub>UTC</sub> (-2450000)	Relative flux	$\sigma_{\text{flux}}$	Inst.
7562.688132	1.014176	0.006391	NGTS
7562.689019	0.993882	0.005278	NGTS
7562.690361	0.993867	0.005867	NGTS
7562.691707	0.997182	0.005817	NGTS
7562.693124	0.992255	0.005179	NGTS
7562.694540	1.001568	0.002645	NGTS
7562.695955	0.990161	0.004289	NGTS
7562.697372	0.991594	0.005725	NGTS
7562.698713	0.991647	0.005552	NGTS
7562.700052	0.992255	0.005312	NGTS

fed by a 2" on-sky science fibre. Radial velocity (RV) measurements were computed for each epoch by cross-correlating with a binary G2 mask (Pepe et al. 2002). The observations showed no significant RV variation within the uncertainties of  $\sim 46 \text{ m s}^{-1}$  and were used to screen NGTS-14A for possible scenarios of blended eclipsing binaries mimicking a planetary transit.

**Table 3.** Radial Velocities for NGTS-14A

BJD <sub>UTC</sub> (-2450000)	RV (m s <sup>-1</sup> )	RV err (m s <sup>-1</sup> )	FWHM (m s <sup>-1</sup> )	BIS (m s <sup>-1</sup> )
8698.71245	30 272.51	4.38	6 147.32	8.36
8699.65656	30 294.53	5.40	6 139.47	5.61
8700.69210	30 299.43	4.63	6 153.15	-1.84
8717.70010	30 298.77	8.05	6 160.60	13.47
8718.60361	30 297.13	4.38	6 161.24	7.71
8719.73729	30 276.65	4.14	6 157.38	11.83
8721.65430	30 302.65	4.81	6 158.79	2.14
8722.60994	30 277.93	4.79	6 140.92	20.31
8723.58722	30 276.65	4.62	6 131.25	10.87
8724.53490	30 295.00	7.17	6 141.78	12.75
8724.80470	30 299.44	5.63	6 120.43	20.12
8725.56246	30 292.16	5.89	6 124.07	4.17
8725.74721	30 287.79	7.45	6 134.53	43.93
8730.60832	30 282.33	7.34	6 131.68	21.46
8746.58959	30 287.98	7.77	6 119.95	8.34

### 3.3.2. HARPS

We observed NGTS-14A using the HARPS spectrograph (Mayor et al. 2003) on ESO’s 3.6-m telescope at La Silla Observatories, Chile, under programmes 0103.C-0719 and 0104.C-0588. A total of fifteen measurements were made between 2019 August 03 and 2019 September 20.

We used the standard HARPS data reduction software to obtain RV measurements of NGTS-14A at each epoch. This was done via cross-correlation with a K5 binary mask. Bisector-span, FWHM and other line-profile diagnostics were computed as well. Using an exposure time of 2700 s we obtained typical error bars of  $\sim 5$  m s<sup>-1</sup>. The resulting radial velocities are listed in Table 3, and are plotted in Fig. 4.

The HARPS science fibre has a 1'' on-sky projection, and does thus not include NGTS-14B. We co-added the fifteen HARPS spectra while weighting each epoch the inverse-variance. Section 4.1 details the spectral analysis performed on the stacked spectrum.

## 4. Stellar characterisation

### 4.1. Spectral analysis

The HARPS spectra were co-added, and the resulting spectrum ( $S/N \approx 49$ ) was analysed with the synthesis method (without the use of wavelets) outlined in Gill et al. (2018). The resulting parameters are  $T_{*,\text{eff}} = 5200 \pm 85$  K,  $[\text{Fe}/\text{H}] = 0.12 \pm 0.08$ ,  $\log g_* = 4.2 \pm 0.1$  (cgs), and  $v \sin i_* = 1.2 \pm 0.5$  km s<sup>-1</sup>.

### 4.2. SED fit with ARIADNE

We fit the spectral energy distribution (SED) of NGTS-14A using ARIADNE, a python tool written to fit catalogue photometry to different atmospheric model grids (Fig. 2). It hosts model grids for Phoenix v2 (Husser et al. 2013), BT-Settl, BT-Cond, BT-NextGen (Allard et al. 2012; Hauschildt et al. 1999), Castelli & Kurucz (2003), and Kurucz (1993) convolved with filter response functions: *UBVRI*; 2MASS *JHK<sub>rms</sub>*; SDSS *ugriz*; WISE *W1* and *W2*; Gaia *G*, *RP*, and *BP*, Pan-STARRS *griwyz*, Strömgren *uvby*; GALEX *NUV* and *FUV*; *TESS*; *Kepler*; and NGTS. Each synthetic SED is modelled by interpolating grids in  $T_{*,\text{eff}}$ - $\log g_*$ - $[\text{Fe}/\text{H}]$  space with the remaining parameters being distance, radius, extinction in the *V* band, and an individual excess

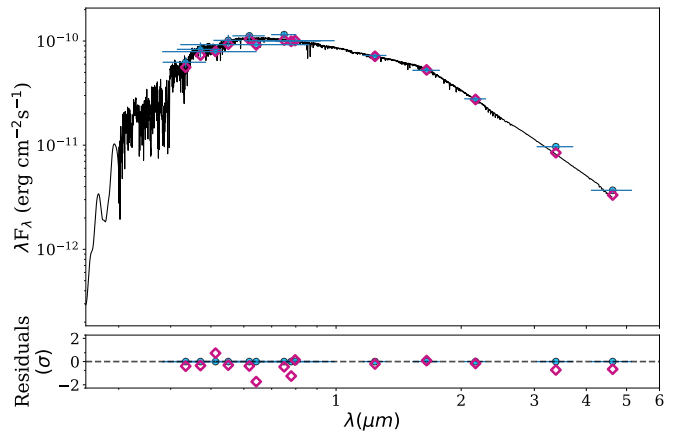


**Fig. 2.** Spectral energy distribution (SED) of NGTS-14A. Catalogue photometric measurements (Table 1) are shown as blue circles, with the horizontal error bars indicating the extent of each bandpass. A model SED from Castelli & Kurucz (2003) is shown as a solid black line, with magenta squares indicating the model flux integrated over each bandpass.

**Table 4.** Stellar parameters

Parameter	Value	Source
$T_{*,\text{eff}}$ / K	$5187 \pm 11$	ARIADNE
$\log g_*$ (cgs)	$4.20 \pm 0.04$	ARIADNE
$v \sin i_*$ / km s <sup>-1</sup>	$1.2 \pm 0.5$	HARPS spectrum
$[\text{Fe}/\text{H}]$	$0.10 \pm 0.03$	ARIADNE
$R_*/R_\odot$	$0.842 \pm 0.006$	ARIADNE
$M_*/M_\odot$	$0.898 \pm 0.035$	ARIADNE
Age / Gyr	$5.9^{+3.0}_{-3.4}$	ARIADNE

noise for each photometry in order to account for underestimated uncertainties. The priors for  $T_{*,\text{eff}}$ ,  $\log g_*$  and  $[\text{Fe}/\text{H}]$  were taken from the spectral analysis determined values, for radius and distance we took the Gaia DR2 reported value, noting that we inflated the radius reported error to account for modelling errors and we applied the Stassun & Torres 2018 correction to the parallax, we limited the  $A_V$  to the maximum line-of-sight taken from the re-calibrated SFD galactic dust map (Schlegel et al. 1998; Schlafly & Finkbeiner 2011), and finally, each excess noise parameter has a zero mean Normal distribution as their priors with a variance equal to five times the size of the reported uncertainty. ARIADNE uses dynesty’s nested sampler for parameter estimation and calculating the Bayesian evidence for each model (Speagle 2020). The final step in ARIADNE’s algorithm is calculating the weighted average of each parameter using the relative probabilities of each models as weights. For a detailed explanation of the fitting procedure, accuracy and precision of ARIADNE the reader is referred to Vines & Jenkins (2020). The resulting stellar parameters are listed in Table 4.

### 4.3. TIC

The TESS Input Catalog (Stassun et al. 2019) lists the following parameters for NGTS-14A, based on the Gaia DR2 (Gaia Collaboration et al. 2018) observations:  $R_* = 0.856 \pm 0.049 R_\odot$ ,  $T_{*,\text{eff}} = 5222 \pm 128$  K. We note that our adopted values are in good agreement with these TIC values.

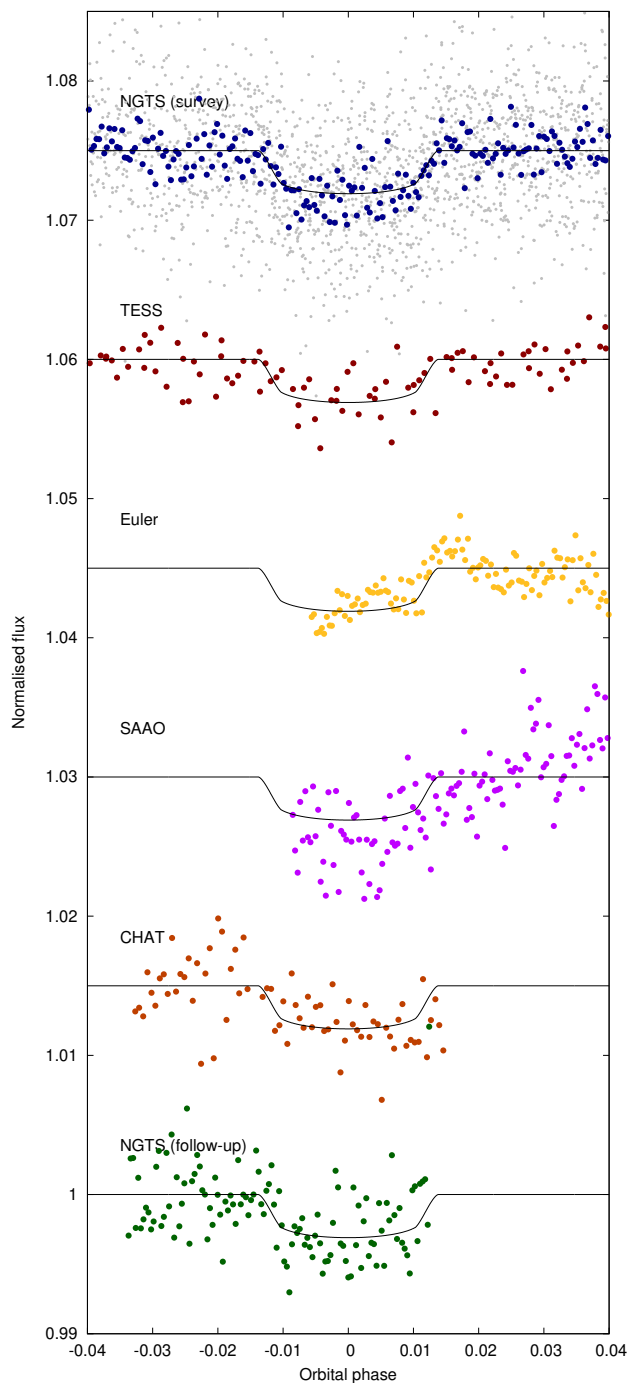


**Fig. 3.** Transit photometry of NGTS-14A from several instruments, offset vertically for clarity. From top-to-bottom: NGTS survey photometry (binned to two minutes in grey, binned to two minutes equivalent in phase in blue); TESS (unbinned); Euler (binned to two minutes); SAAO (binned to two minutes); CHAT (unbinned); single night NGTS multi-telescope observations (binned to two minutes). Our best-fitting model is shown as a solid black line.

#### 4.4. Stellar rotation

We searched the NGTS survey light curve for periodic signals, using both a Lomb-Scargle periodogram and a generalised autocorrelation (G-ACF) method (Gillen et al. 2020). Both methods revealed a signal with a period of approximately 10 d to be the most prominent, although given the small amplitude of the putative signal ( $\leq 1$  mmag), this is not a robust detection.

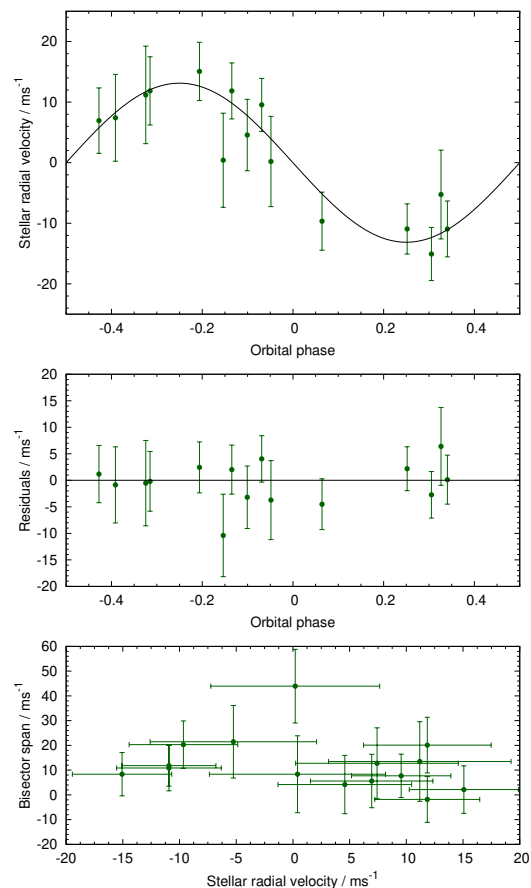


**Fig. 4.** Radial velocities of NGTS-14A from HARPS. Upper panel: RV as a function of orbital phase, with best-fitting model shown as a solid black line. Middle panel: residuals to the best-fitting model. Lower panel: bisector span of the stellar lines against radial velocity. The uncertainties on the bisector spans are taken to be twice the uncertainty on the radial velocities.

From the  $v \sin i_*$  derived from the HARPS spectra ( $1.2 \pm 0.5 \text{ km s}^{-1}$ ) and the stellar radius, we calculate an upper limit to the stellar rotation period,  $P_{*,\text{rot}} \leq 35.5 \pm 14.8 \text{ d}$ . This value corresponds to the case where the stellar spin and planet rotation axes are aligned.

It is unclear if the 10-d signal is related to rotation, since it would imply a faster-rotating star than suggested by the  $v \sin i_*$ , and would be indicative of a star significantly younger (c. 700 Myr; Rebull et al. 2017; Douglas et al. 2017) than our SED analysis (Sec. 4.2) implies. At an age less than 1 Gyr, K0 stars typically exhibit photometric rotational modulation of at least a few mmag, which would be readily detectable in the NGTS data.

## 5. Joint fit to photometry and RVs

We performed a joint fit to the photometry and radial velocities using the Transit and Light Curve Modeller (TLCM; Csizmadia 2020). In order to reduce the large number of data points in the NGTS survey photometry, and thus increase modelling speed, we modelled only those nights of NGTS data where a transit occurred, and we binned the remaining light curve to a cadence of 120 s. This resulted in a total of 2404 NGTS survey data points. Similarly, the NGTS multi-telescope data were binned to a single light curve with a cadence of 120 s. We excluded TESS data taken far from transit, only modelling that with an orbital phase

between -0.1 and 0.1. The CHAT, SAAO, and Euler light curves were modelled unbinned and in their entirety.

### 5.1. Contaminating flux from NGTS-14B

In all photometric data sets, except that from the SAAO 1-m, NGTS-14B (Sec. 2) is well within the photometric aperture used to extract the target flux from the images. To account for this contamination, we calculated the flux ratio of the two components of NGTS-14, and corrected the affected datasets accordingly. We find that NGTS-14B contributes around two per cent of the observed flux, and that in the absence of any correction, our value of  $R_p/R_*$  is biased by around  $2\sigma$ .

### 5.2. Stellar limb darkening

The signal-to-noise ratio of our photometry is not sufficiently high to precisely constrain the limb-darkening coefficients in each bandpass in which we observed NGTS-14A. The bandpasses used do not span a particularly large range of wavelengths; rather they are fairly similar to each other. We calculated theoretically expected quadratic limb-darkening coefficients for each band using the Limb Darkening Toolkit (LDTk) of Parviainen & Aigrain (2015), which relies on the stellar models of Husser et al. (2013). The difference between the coefficients for the different bandpasses is insignificant, much smaller than the uncertainties on the coefficients we measure for each light curve individually. Further, we find that our derived system parameters are insensitive to our choice of limb-darkening parameters, within this range. We therefore opt to fit for a single pair of limb-darkening coefficients, common to all observed bandpasses. In TLMCM, this is done with the parameters  $u_+ = u_a + u_b$  and  $u_- = u_a - u_b$ , where  $u_a$  and  $u_b$  are the commonly used quadratic coefficients.

### 5.3. Orbital eccentricity

We also tried fitting for an eccentric orbit, via the additional parameters  $\sqrt{e} \sin(\omega)$  and  $\sqrt{e} \cos(\omega)$ , where  $e$  is the orbital eccentricity, and  $\omega$  the argument of periastron. Our best-fitting values are  $\sqrt{e} \sin(\omega) = 0.07 \pm 0.27$  and  $\sqrt{e} \cos(\omega) = -0.05 \pm 0.20$ , resulting in  $e = 0.0074 \pm 0.0428$  and  $\omega = -54 \pm 151$  degrees. The three-sigma upper limit to the eccentricity is 0.11. The very modest improvement in  $\chi^2$  of less than 0.4 does not compensate for the much larger Bayesian penalty on having two additional model parameters. This results in a significantly lower BIC (Bayesian Information Criterion) for the circular orbital model ( $\Delta \text{BIC}_{\text{circ-ecc}} = -5.05$ ). We therefore reject the eccentric model, and adopt  $e = 0$ .

### 5.4. Additional trend in RVs

We also tried fitting for a radial acceleration,  $\dot{\gamma}$ , of NGTS-14A. The presence of such a trend in the RVs is usually indicative of an additional body in the system (e.g. Smith et al. 2017). We obtained a best-fitting value  $\dot{\gamma} = -9_{-17}^{+21} \text{ m s}^{-1} \text{ yr}^{-1}$ , suggesting that no significant radial acceleration is detected. This is confirmed by a BIC analysis, where the simpler model with no acceleration has a smaller BIC value (by 1.2), and is hence preferred.

### 5.5. Bisector spans

We observe no evidence for a correlation between either time and bisector span or bisector span and radial velocity (Fig. 4). A correlation can indicate that the apparent planetary signal is caused by a blended eclipsing binary system, or by stellar activity (Queloz et al. 2001a). Furthermore, we see no correlation between radial velocity and the FWHM of the line profile.

Our joint fit to the photometry and RVs is shown in Figs. 3 and 4, respectively. The resulting system parameters are listed in Table 5.

## 6. Discussion

### 6.1. NGTS-14Ab in the Neptunian desert

NGTS-14Ab joins a growing number of planets that reside in the Neptunian desert, a sparsely populated region of parameter space between the hot Jupiters and the super Earths in the radius – period plane (Fig. 5). NGTS-14Ab lies within both the desert as defined by Mazeh et al. (2016), and the smaller region identified by Szabó & Kálmán (2019), who along with Eigmüller et al. (2019) have recently investigated the boundaries of the Neptunian desert as a function of host star spectral type.

Owen & Lai (2018) explain the lower boundary of the desert as a consequence of photoevaporation – a process that is more efficient at reducing the size of close-in planets. Further, they suggest that the upper boundary of the desert is a result of the fact that only the highest mass planets can be tidally circularised in the closest orbits, after high-eccentricity migration. NGTS-14Ab lies among the lower boundaries of the desert computed by Owen & Lai (2018), which are dependent upon metallicity and core mass. Comparing NGTS-14Ab to their simulations (which ran for 5 Gy, similar to the age of the system) suggests that NGTS-14Ab has a core mass of close to  $10 M_{\oplus}$ , and that any additional envelope accreted by the planet during its formation would have by now been lost to photoevaporation.

We use the neural network model of planetary interiors developed by Baumeister et al. (2020) to predict the internal structure of NGTS-14Ab (Fig. 6), using the planetary mass and radius (Table 5) as model inputs. Although internal structure is notoriously degenerate with mass and radius, this model suggests that NGTS-14Ab has a significant gaseous envelope. The models of Howe et al. (2014) suggest that an  $\text{H}_2$ -He envelope constituting approximately half of the planet’s radius would contribute five to ten per cent of the planet’s mass, for a core mass of  $10 M_{\oplus}$ . In other words, there is broad compatibility between the models of Baumeister et al. (2020) (Fig. 6) and the model of Zeng et al. (2019) with a five per cent (by mass) hydrogen-rich envelope (Fig. 7, red curve).

In Fig. 7, we compare NGTS-14Ab to the other planets that inhabit ‘Region A’ of Szabó & Kálmán (2019), i.e. those planets having radii between 0.28 and  $0.63 R_{\text{Jup}}$ . Planets orbiting closer than NGTS-14Ab does, such as NGTS-4 b (West et al. 2019) and TOI-132 b (Díaz et al. 2020), tend to be denser because they have undergone evaporation, and lost much or all of their primary, hydrogen-dominated atmospheres. The most extreme example of this is the recently-discovered TOI-849 b (Armstrong et al. 2020), thought to be the remnant core of a giant planet. LTT 9779 b (Jenkins et al. 2020) on the other hand, remains an intriguing exception – how it has apparently retained its hydrogen-rich envelope is a mystery. NGTS-14Ab appears to just far enough from its star that it is able to maintain a significant atmosphere, resulting in a density similar to those of Uranus and Neptune.

**Table 5.** Parameters from light curve and RV data analysis.

Parameter	value	unit
TLCM fitted parameters:		
Orbital period $P_{\text{orb}}$	$3.5357173 \pm 0.0000069$	d
Transit epoch $T_0$	$7502.5545 \pm 0.0020$	BJD <sub>TDB</sub> – 2450000
Scaled semi-major axis $a/R_*$	$10.3^{+2.3}_{-2.6}$	
Radius ratio $R_p/R_*$	$0.0530^{+0.0038}_{-0.0033}$	
Transit impact parameter $b$	$0.59^{+0.23}_{-0.38}$	
Limb-darkening coefficient $u_+$	$0.65 \pm 0.19$	
Limb-darkening coefficient $u_-$	$0.30 \pm 0.21$	
Radial velocity semi amplitude $K$	$13.2 \pm 1.7$	$\text{m s}^{-1}$
Systemic radial velocity $\gamma$	$30.2876 \pm 0.0013$	$\text{km s}^{-1}$
Derived parameters:		
Eccentricity $e$	0.0	(fixed, see Sec. 5.3)
Semi-major axis $a$	$0.0403 \pm 0.0071$	au
Orbital inclination angle $i$	$86.7 \pm 1.7$	deg
Transit Duration $T_{14}$	$2.24^{+0.08}_{-0.06}$	h
Planet mass $M_p$	$0.092 \pm 0.012$	$M_{\text{Jup}}$
Planet radius $R_p$	$0.444 \pm 0.030$	$R_{\text{Jup}}$
Planet mean density	$1395 \pm 333$	$\text{kg m}^{-3}$
Planet surface gravity $\log g_p$	$3.08 \pm 0.08$	(cgs)
Planet equilibrium temperature <sup>†</sup> $T_{\text{p,A}=0}$	$1143 \pm 139$	K

<sup>†</sup> assuming zero albedo, and isotropic heat redistribution.

## 6.2. Stellar companion

Motivated by the apparent stellar companion to NGTS-14A (Section 2), and NGTS-14Ab’s position in the Neptunian desert (as defined by Mazeh et al. 2016), we conducted a search for stellar companions to other planet host stars in and around the desert. The presence of a long-period companion may influence the evolution of a planetary system, for instance by driving high-eccentricity migration (Wu & Murray 2003).

We used the Gaia DR2 catalogue Gaia Collaboration et al. (2018) to search for companions to stars that are listed in the NASA Exoplanet Archive<sup>4</sup> as hosting planets with orbital periods less than ten days, and masses measured to a precision of less than 50 per cent. We then sub-divided the sample into planets lying above, in, or below the Neptunian desert (as defined in the mass-period plane in Mazeh et al. 2016). This resulted in 73 systems in the desert, 339 systems above the desert, and 55 systems (70 planets) below the desert.

We then queried Gaia DR2, using a cone search centred on each object, conducted using the astroquery package (Ginsburg et al. 2019). The radius of the search was chosen individually for each object, so that it corresponds to a separation of 10 000 au. We then applied the same technique as used in Section 2 to search for nearby objects whose parallaxes and proper motions match the planet host star within  $n\sigma$ . For  $n = 3$ , we identified possible companions to 62 host stars (18.3 per cent) from above the desert, ten (13.7 per cent) in the desert, and three (5.5 per cent) below it. Combining the results for above and below the desert, we find potential companions to 16.5 per cent of host stars outside the desert, which is statistically indistinguishable from the proportion inside the desert. These results are summarised in Table 6.

<sup>4</sup> <https://exoplanetarchive.ipac.caltech.edu/>, accessed 2020 June 17.

To extend our binarity analysis to companions too close to be resolved as individual objects in Gaia DR2, we used the renormalized unit weight error (RUWE) to the Gaia DR2 astrometric solutions (Lindegren et al. 2018). A previous analysis conducted using the RUWE statistic has suggested that there is tentative evidence for increased binarity among hot Jupiter host stars (Belokurov et al. 2020).

We adopt the threshold of  $\text{RUWE} = 1.4$  suggested by the Gaia team for distinguishing between well-behaved solutions and those where an unseen additional body may impact the astrometry<sup>5</sup>. In Table 6, we report the number of systems for which the RUWE statistic is greater than 1.4. We fail to find a significant difference between the RUWE distributions for objects inside and outside the Neptunian desert. There is, however, a hint of fewer companions below the desert, with no large RUWE values in this population.

Finally, we attempted to compare the three populations of exoplanet-hosting stars with their non-exoplanet host counterparts. To do this, for each exoplanet host star, we searched Gaia DR2 for other nearby stars with similar properties. Specifically, we required that the  $G$ -band magnitude be within 0.25, the  $G_{\text{BP}} - G_{\text{RP}}$  colour within 15 per cent, and the parallax within a factor 2 (to exclude giant stars). Where multiple stars were found to match these criteria, we selected one at random. We then performed the same analysis on these non-exoplanet host stars as on the hosts; the results are reported in the lower part of Table 6.

We see fewer potential long-period companions with matching parallax and proper motions amongst the non-host stars, suggesting that the presence of a long-period companion increases the probability of a star hosting an exoplanet in or above the desert. Non-well behaved ( $\text{RUWE} > 1.4$ ) astrometric solutions are more likely to occur around stars not known to host an ex-

<sup>5</sup> Technical note GAIA-C3-TN-LU-LL-124-01 [http://www.rssd.esa.int/doc\\_fetch.php?id=3757412](http://www.rssd.esa.int/doc_fetch.php?id=3757412)

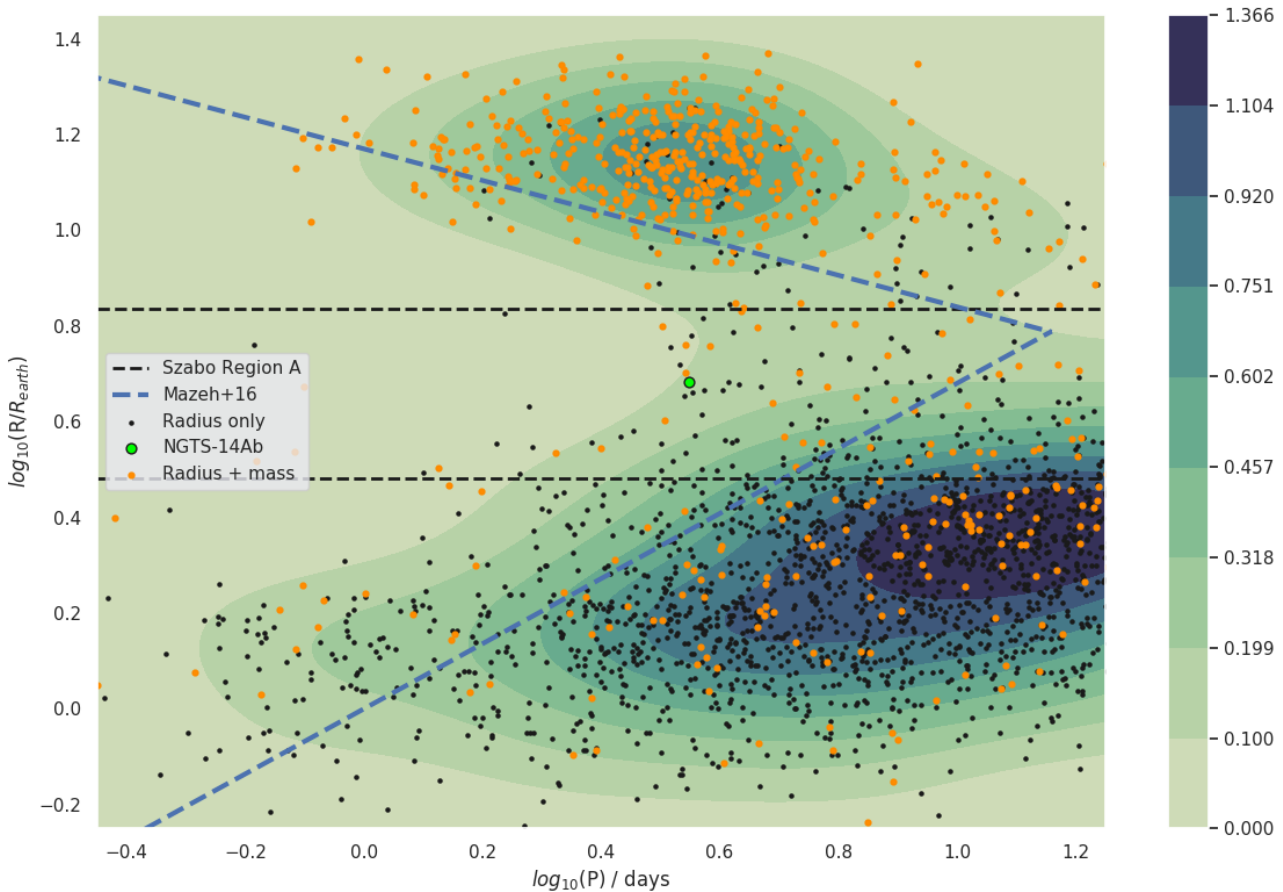


**Fig. 5.** NGTS-14Ab (light green point) within the Neptunian desert, the boundary of which (as defined by Mazeh et al. 2016) is indicated with blue dashed lines. The black dashed lines indicate the region of interest identified by Szabó & Kálmán (2019). The parameters of other planets come from the NASA Exoplanet Archive, and the colour scale indicates the number of planets per grid element. The plot comprises  $200 \times 200$  elements, uniformly spaced in  $\log_{10} P$  and  $\log_{10} R$ .

**Table 6.** Potential companions to planetary host stars, based on analysis of Gaia DR2 data. ‘Plx & PM matches’ refers to potential long-period companions identified by their matching parallaxes and proper motions. ‘RUWE > 1.4’ refers to stars whose astrometric fits exhibit excess noise, potentially indicating the presence of a binary companion.

	Subset	No. of systems	Plx & PM matches		RUWE > 1.4	
			No.	%	No.	%
Exoplanet host stars						
	Desert	73	10	13.7	4	5.5
	Above desert	339	62	18.3	18	5.3
	Below desert	55	3	5.5	0	0.0
	Above + below	394	65	16.5	18	4.6
	Sum of all host stars	467	75	15.6	22	4.6
Analogous non-host stars						
	Desert	73	1	1.4	11	15.1
	Above desert	339	27	8.0	49	14.5
	Below desert	55	5	9.1	14	25.5
	Sum of all non-host stars	467	33	7.1	74	15.8

oplanet, perhaps indicating that short-period binaries are more common in this population. We note, however, that selection effects may play a role here, in that short-period binarity of an exoplanet candidate host star may complicate both photometric and spectroscopic follow-up, and hence the confirmation of exoplanets orbiting stars with close binary companions.

Although this binarity analysis is inconclusive, future Gaia data releases will include the identification of further gravitation-

ally bound companions to exoplanet host stars. This may allow any trends with planet parameters (such as membership of the Neptunian desert) to be elucidated.

## 7. Conclusions

We have presented the discovery of the NGTS-14 system, which consists of an early K-type dwarf star, NGTS-14A, with a long-

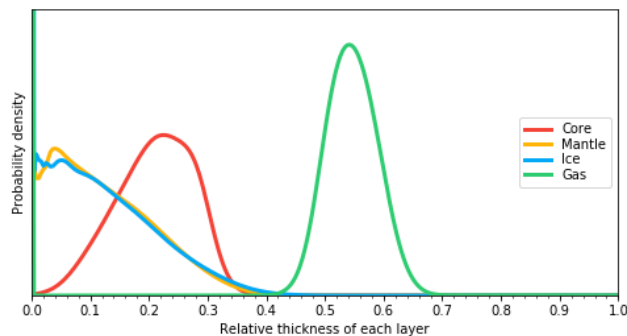


**Fig. 6.** Possible internal structure for NGTS-14Ab, the result of the neural network model of Baumeister et al. (2020). Shown are the predictions of the relative interior layer thicknesses, using our derived planetary mass and radius as inputs. The colored lines show the combined Gaussian mixture prediction of the model, with the area under each curve normalised to unity.

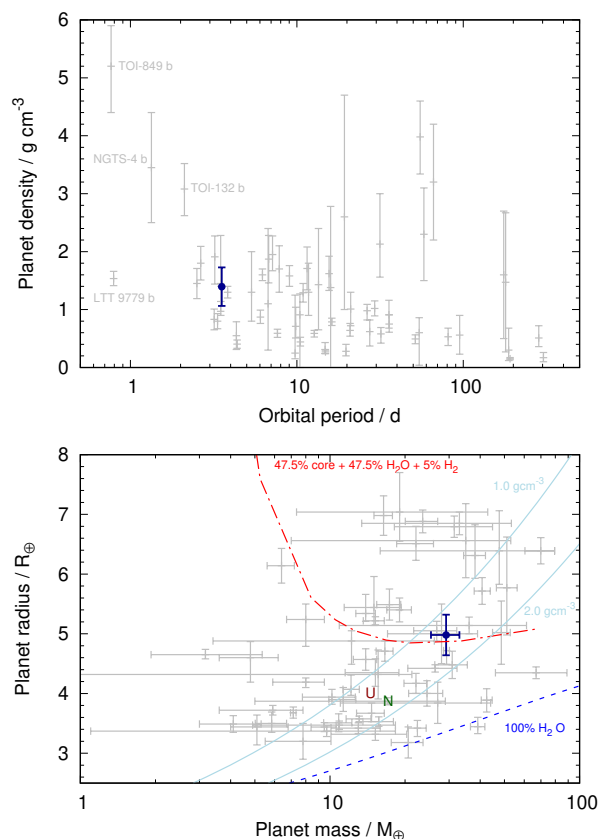


**Fig. 7.** NGTS-14Ab compared to other planets within the Neptunian desert, as defined by Szabó & Kálmán (2019) (their ‘Region A’ – the area between the dashed black lines in Fig. 5). Planetary data is taken from the NASA Exoplanet Archive. NGTS-14Ab is denoted by a dark blue point in both panels. Upper panel: Planet density versus orbital period. Several planets discussed in the text are labelled with their names. Lower panel: planet radius versus mass. The Solar System ice giants are indicated with their initial letters, and lines of constant density ( $1.0 \text{ g cm}^{-3}$  and  $2.0 \text{ g cm}^{-3}$ ) are shown with solid pale blue lines. Two models from Zeng et al. (2019) corresponding to compositions of pure water (dashed blue line) and an Earth-like rocky core with an equal mass of water, and five per cent hydrogen (dash-dotted red line) are also shown.

period companion, NGTS-14B, which is likely to be a mid-M dwarf. The primary star is orbited by a transiting exoplanet, NGTS-14Ab, which is slightly larger and more massive than Neptune. The planet’s orbital period of just over 3.5 days places it in the Neptunian desert, a thus far sparsely-populated region of parameter space. NGTS-14Ab has a density which suggests that it has retained some of its primordial atmosphere.

*Acknowledgements.* This work uses data collected under the NGTS project at the ESO La Silla Paranal Observatory. The NGTS facility is operated by the consortium institutes with support from the UK Science and Technology Facilities Council (STFC) under projects ST/M001962/1 and ST/S002642/1. This research made use of Astropy,<sup>6</sup> a community-developed core Python package for Astronomy (Astropy Collaboration et al. 2013; Price-Whelan et al. 2018). This work has made use of data from the European Space Agency (ESA) mission *Gaia* (<https://www.cosmos.esa.int/gaia>), processed by the *Gaia* Data Processing and Analysis Consortium (DPAC, <https://www.cosmos.esa.int/web/gaia/dpac/consortium>). Funding for the DPAC has been provided by national institutions, in particular the institutions participating in the *Gaia* Multilateral Agreement. This research has made use of the NASA Exoplanet Archive, which is operated by the California Institute of Technology, under contract with the National Aeronautics and Space Administration under the Exoplanet Exploration Program. This publication makes use of data products from the Wide-field Infrared Survey Explorer, which is a joint project of the University of California, Los Angeles, and the Jet Propulsion Laboratory/California Institute of Technology, funded by the National Aeronautics and Space Administration. This study is based on observations collected at the European Southern Observatory under ESO programmes 0103.C-0719 and 0104.C-0588.

We thank the Swiss National Science Foundation (SNSF) and the Geneva University for their continuous support to our planet search programs. This work has been in particular carried out in the frame of the National Centre for Competence in Research *PlanetS* supported by the Swiss National Science Foundation (SNSF).

This publication makes use of The Data & Analysis Center for Exoplanets (DACE), which is a facility based at the University of Geneva (CH) dedicated to extrasolar planets data visualisation, exchange and analysis. DACE is a platform of the Swiss National Centre of Competence in Research (NCCR) *PlanetS*, federating the Swiss expertise in Exoplanet research. The DACE platform is available at <https://dace.unige.ch>.

MNG acknowledges support from MIT’s Kavli Institute as a Juan Carlos Torres Fellow. Contributions by authors from the University of Warwick were supported by STFC consolidated grants ST/P000495/1 and ST/T000406/1. DJA acknowledges support from the STFC via an Ernest Rutherford Fellowship (ST/R00384X/1). EG gratefully acknowledges support from the David and Claudia Harding Foundation in the form of a Winton Exoplanet Fellowship. Ph.E., A.C., and H.R. acknowledge the support of the DFG priority program SPP 1992 ‘‘Exploring the Diversity of Extrasolar Planets’’ (RA 714/13-1). R.B. acknowledges support from FONDECYT Post-doctoral Fellowship Project 3180246, and from the Millennium Institute of Astrophysics (MAS).

Finally, we acknowledge our anonymous referee, whose comments helped to improve the quality of this manuscript.

## References

- Allard, F., Homeier, D., & Freytag, B. 2012, *Philosophical Transactions of the Royal Society A: Mathematical, Physical and Engineering Sciences*, 370, 2765
- Armstrong, D. J., Lopez, T. A., Adibekyan, V., et al. 2020, *Nature*, 583, 39
- Astropy Collaboration, Robitaille, T. P., Tollerud, E. J., et al. 2013, *A&A*, 558, A33
- Bakos, G. Á., Lázár, J., Papp, I., Sári, P., & Green, E. M. 2002, *PASP*, 114, 974
- Barbary, K. 2016, *Journal of Open Source Software*, 58
- Baumeister, P., Padovan, S., Tosi, N., et al. 2020, *ApJ*, 889, 42
- Belokurov, V., Penoyre, Z., Oh, S., et al. 2020, *MNRAS*, 496, 1922
- Bertin, E. & Arnouts, S. 1996, *A&AS*, 117, 393
- Borucki, W. J., Koch, D., Basri, G., et al. 2010, *Science*, 327, 977
- Bryant, E. M., Bayliss, D., McCormac, J., et al. 2020, *MNRAS*, 494, 5872
- Castelli, F. & Kurucz, R. L. 2003, in *Modelling of Stellar Atmospheres*, ed. N. Piskunov, W. W. Weiss, & D. F. Gray, Vol. 210, A20
- Chaushev, A., Raynard, L., Goad, M. R., et al. 2019, *MNRAS*, 488, 5232
- Collier Cameron, A., Pollacco, D., Street, R. A., et al. 2006, *MNRAS*, 373, 799
- Coppejans, R., Gulbis, A. A. S., Kotze, M. M., et al. 2013, *PASP*, 125, 976
- Csizmadia, S. 2020, *MNRAS*, 496, 4442
- Cutri, R. M. & et al. 2013, *VizieR Online Data Catalog*, II/328

<sup>6</sup> <http://www.astropy.org>

- Díaz, M. R., Jenkins, J. S., Gandolfi, D., et al. 2020, *MNRAS*, 493, 973
- Douglas, S. T., Agüeros, M. A., Covey, K. R., & Kraus, A. 2017, *ApJ*, 842, 83
- Eigmüller, P., Chaushev, A., Gillen, E., et al. 2019, *A&A*, 625, A142
- Espinoza, N., Hartman, J. D., Bakos, G. Á., et al. 2019, *AJ*, 158, 63
- Gaia Collaboration, Brown, A. G. A., Vallenari, A., et al. 2018, *A&A*, 616, A1
- Gaia Collaboration, Prusti, T., de Bruijne, J. H. J., et al. 2016, *A&A*, 595, A1
- Gill, S., Maxted, P. F. L., & Smalley, B. 2018, *A&A*, 612, A111
- Gillen, E., Briegal, J. T., Hodgkin, S. T., et al. 2020, *MNRAS*, 492, 1008
- Ginsburg, A., Sipőcz, B. M., Brasseur, C. E., et al. 2019, *AJ*, 157, 98
- Günther, M. N., Queloz, D., Gillen, E., et al. 2017, *MNRAS*, 472, 295
- Hartman, J. D., Bakos, G. Á., Bayliss, D., et al. 2019, *AJ*, 157, 55
- Hauschildt, P. H., Allard, F., & Baron, E. 1999, *ApJ*, 512, 377
- Henden, A. A., Templeton, M., Terrell, D., et al. 2016, *VizieR Online Data Catalog*, II/336
- Howe, A. R., Burrows, A., & Verne, W. 2014, *ApJ*, 787, 173
- Howell, S. B., Sobeck, C., Haas, M., et al. 2014, *PASP*, 126, 398
- Husser, T.-O., Wende-von Berg, S., Dreizler, S., et al. 2013, *A&A*, 553, A6
- Jenkins, J. S., Díaz, M. R., Kurtovic, N. T., et al. 2020, *Nature Astronomy* [arXiv:2009.12832]
- Jiang, Y.-F. & Tremaine, S. 2010, *MNRAS*, 401, 977
- Jordán, A., Brahm, R., Espinoza, N., et al. 2019, *AJ*, 157, 100
- Kovács, G., Zucker, S., & Mazeh, T. 2002, *A&A*, 391, 369
- Kurucz, R. L. 1993, *VizieR Online Data Catalog*, 6039
- Lindegren, L., Hernández, J., Bombrun, A., et al. 2018, *A&A*, 616, A2
- Mayor, M., Pepe, F., Queloz, D., et al. 2003, *The Messenger*, 114, 20
- Mazeh, T., Holczer, T., & Faigler, S. 2016, *A&A*, 589, A75
- McCormac, J., Pollacco, D., Skillen, I., et al. 2013, *PASP*, 125, 548
- Owen, J. E. & Lai, D. 2018, *MNRAS*, 479, 5012
- Parviainen, H. & Aigrain, S. 2015, *MNRAS*, 453, 3821
- Pecaut, M. J. & Mamajek, E. E. 2013, *ApJS*, 208, 9
- Pepe, F., Mayor, M., Rupprecht, G., et al. 2002, *The Messenger*, 110, 9
- Pollacco, D. L., Skillen, I., Cameron, A. C., et al. 2006, *PASP*, 118, 1407
- Price-Whelan, A. M., Sipőcz, B. M., Günther, H. M., et al. 2018, *AJ*, 156, 123
- Queloz, D., Henry, G. W., Sivan, J. P., et al. 2001a, *A&A*, 379, 279
- Queloz, D., Mayor, M., Udry, S., et al. 2001b, *The Messenger*, 105, 1
- Rebull, L. M., Stauffer, J. R., Hillenbrand, L. A., et al. 2017, *ApJ*, 839, 92
- Ricker, G. R., Winn, J. N., Vanderspek, R., et al. 2015, *Journal of Astronomical Telescopes, Instruments, and Systems*, 1, 014003
- Schlafly, E. F. & Finkbeiner, D. P. 2011, *Astrophysical Journal*, 737
- Schlegel, D. J., Finkbeiner, D. P., & Davis, M. 1998, *ApJ*, 500, 525
- Sestovic, M., Demory, B.-O., & Queloz, D. 2018, *A&A*, 616, A76
- Sing, D. K., Fortney, J. J., Nikolov, N., et al. 2016, *Nature*, 529, 59
- Skrutskie, M. F., Cutri, R. M., Stiening, R., et al. 2006, *AJ*, 131, 1163
- Smith, A. M. S., Eigmüller, P., Gurumoorthy, R., et al. 2020, *Astronomische Nachrichten*, 341, 273
- Smith, A. M. S., Gandolfi, D., Barragán, O., et al. 2017, *MNRAS*, 464, 2708
- Speagle, J. S. 2020, *MNRAS*, 493, 3132
- Stassun, K. G., Oelkers, R. J., Paegert, M., et al. 2019, *AJ*, 158, 138
- Stassun, K. G. & Torres, G. 2018, *ApJ*, 862, 61
- Szabó, G. M. & Kálmán, S. 2019, *MNRAS*, 485, L116
- Szabó, G. M. & Kiss, L. L. 2011, *ApJ*, 727, L44
- Tamuz, O., Mazeh, T., & Zucker, S. 2005, *MNRAS*, 356, 1466
- Thorngren, D. P. & Fortney, J. J. 2018, *AJ*, 155, 214
- Vines, J. I. & Jenkins, J. S. 2020, in prep
- West, R. G., Gillen, E., Bayliss, D., et al. 2019, *MNRAS*, 486, 5094
- Wheatley, P. J., West, R. G., Goad, M. R., et al. 2018, *MNRAS*, 475, 4476
- Wu, Y. & Murray, N. 2003, *ApJ*, 589, 605
- Zeng, L., Jacobsen, S. B., Sasselov, D. D., et al. 2019, *Proceedings of the National Academy of Science*, 116, 9723